Molecular Structure of Monomorphic Peptide Fibrils within a Kinetically Trapped Hydrogel Network

Katelyn Nagy-Smith, Eric Moore, Joel Schneider, and Robert Tycko

Supporting Information, consisting of Supporting Methods, Tables S1 and S2, and Figures S1 through S8

Supporting Methods

Peptide synthesis and purification

PL-Rink amide resin was purchased from Polymer Laboratories. Fmoc-protected valine, threonine, and L- and D-proline were purchased through EMD Chemicals. Fmoc-protected lysine was purchased from Bachem. Isotopically labeled amino acids were purchased from Cambridge Isotopes or Anaspec. Diisopropylethylamine, methanol, acetic anhydride, piperidine, 1,8-Diazabicyclo[5.4.0]undec-7-ene (DBU), and spectroscopic grade trifluoroacetic acid (TFA) were purchased through Sigma-Aldrich. 2-(6-Chloro-1H-benzotriazole-1-yl)-1,1,3,3-tetramethylaminium hexafluorophosphate (HCTU) was purchased from Peptides International. N-methylpyrolidinone, acetonitrile, dimethylformamide (DMF), trifluoroacetic acid, thioanisole, ethanedithiol, anisole, BIS-TRIS propane (BTP), ethylenediaminetetraacetic acid (EDTA), sodium chloride (NaCl), diethyl ether, and hydrochloric acid were purchased through Fisher.

All isotopically labeled MAX1 derivatives were synthesized using standard Fmoc solid phase peptide synthesis with HCTU activation on an ABI 433A or Tribute (Protein Technologies Inc.) automated peptide synthesizer. Resin bound peptide was cleaved and side-chain deprotected using trifluoroacetic acid/thioanisole/ethanedithiol/anisole (90:5:3:2) for two hours under inert gas. Crude peptides were precipitated with cold diethyl ether after separation of resin by filtration. The resulting crude peptides were purified by RP-HPLC (Vydac C18 Column) at 40°C using an isocratic gradient from 0 – 2 minutes at 0% standard B, then utilizing a linear gradient from 0 – 15% standard B for 8 minutes followed by a gradient of 15 – 100% standard B over 149 minutes. Here, standard A is 0.1% TFA in water and standard B is 90% MeCN, 9.9% H_2O, and 0.1% TFA. Peptides elute at 36 minutes. Purified peptide solutions were lyophilized, resulting in pure peptide powders that were utilized in hydrogel formation. Purity of each peptide was confirmed by analytical HPLC and positive mode electrospray ionization-mass spectrometry. Analytical HPLC chromatograms were collected by monitoring 200 nm with a gradient of 0-100 % standard B over 100 minutes.

Hydrogel preparation

2 wt % hydrogels were formed and then lyophilized, affording solid, dry fibrillar "lyo-gels" which were used for NMR measurements. Briefly, 6 mg of pure peptide powder was dissolved in 150 µl milli-pure water to afford a 4 wt % peptide stock solutions. Gelation was initiated via the addition of an equal volume of buffer containing 250 mM BTP and 20 mM NaCl at pH 9 resulting in 300 µl of a 2 wt % peptide solution (125 mM BTP, 10 mM NaCl at pH 9) that quickly gelled. 2 wt % hydrogels were allowed to form at room temperature for at least 2

hours. Hydrogels were then frozen by liquid nitrogen and lyophilized. The resulting "lyo-gels" were then used in subsequent solid state NMR experiments either in a dry or rehydrated state.

Solid state NMR

Data were acquired on three spectrometers, namely a Varian InfinityPlus operating at 100.4 MHz ^{13}C NMR frequency (399.2 MHz ^{1}H NMR frequency), a Bruker Avance III operating at 100.8 MHz ^{13}C NMR frequency (400.9 MHz ^{1}H NMR frequency), and a Varian Infinity operating at 187.8 MHz ^{13}C NMR frequency (746.8 MHz ^{1}H NMR frequency). A triple-resonance Varian MAS probe with 3.2 mm rotors was used at 100.4 MHz and 100.8 MHz. A triple-resonance MAS probe from the laboratory of Dr. Ago Samoson (NMR Institute, Tallinn Technical University) with 1.8 mm rotors was used at 187.8 MHz.

Measurements of ^{15}N-^{13}C magnetic dipole-dipole couplings in samples I-IV were performed at 100.4 MHz ^{13}C NMR frequency with the rotational echo double resonance (REDOR) technique (1, 2), using a 9.00 kHz MAS frequency, one ^{15}N and one ^{13}C π pulse per rotation period τ_R with pulse lengths of 16.7 μs and 10.0 μs, and 100 kHz ^{1}H decoupling during the REDOR period. Pulses were actively synchronized with the MAS tachometer signal. Pulse sequences for S_0 and S_1 REDOR signals differed by the absence or presence, respectively, of the ^{15}N π pulse train. ^{13}C NMR signals were detected with pulsed spin locking (PSL) to enhance sensitivity (3), with 80 kHz ^{1}H decoupling during detection. Experimental data in Figs. 3a, S2a, and S3a are REDOR difference signals, *i.e.*, $(S_0 - S_1)/S_0$. Typically, a complete REDOR data set for one sample required 14-24 h of signal acquisition, with a 2.0 s recycle delay and with the number of scans increasing in proportion to the REDOR dephasing period.

Measurements of ^{13}C-^{13}C magnetic dipole-dipole couplings in samples I-VIII were performed at 100.4 MHz and 100.8 MHz ^{13}C NMR frequencies with the constant-time, $\tau_R/3$ π-pulse recoupling (PITHIRDS-CT) technique as previously described (4), using 20.00 kHz MAS, active synchronization, and PSL detection. ^{1}H decoupling fields were 100 kHz during PITHIRDS-CT periods and 75-85 kHz during signal detection. A complete PITHIRDS-CT data set for one sample was acquired in 18-24 h, with a 3 s recycle delay.

Measurement of intramolecular ^{15}N-^{15}N couplings among backbone amide nitrogens and ^{13}C-^{13}C couplings among backbone carbonyl sites in sample IX were performed with the ^{15}N and ^{13}C backbone recoupling (^{15}N-BARE and ^{13}C-BARE) techniques (5). ^{15}N-BARE data were acquired at 100.4 MHz ^{13}C NMR frequency, using 9.00 kHz MAS, active synchronization, and 106 kHz ^{1}H decoupling. Decay curves for ^{15}N sites of V9, P11, T12, and K13 were detected through signals of V9 C_α, P11 C_γ, T12 C_β, and K13 C_α in one-dimensional ^{13}C NMR spectra. These ^{13}C sites were polarized by a 4.0 ms ^{15}N-$^{13}C_\alpha$ cross-polarization period and a 3.0 ms ^{13}C-^{13}C exchange period after the ^{15}N-^{15}N dipolar recoupling period of the ^{15}N-BARE sequence. ^{15}N-BARE data were acquired in 93 h, with a 3.5 s recycle delay. ^{13}C-BARE data were acquired at 187.8 MHz ^{13}C NMR frequency, using 40.00 kHz MAS, active synchronization and 100 kHz ^{1}H decoupling during signal acquisition but no decoupling during the ^{13}C-^{13}C dipolar recoupling period. Chemical shift evolution periods of 75 μs and Gaussian π pulses with lengths of 250 μs were used to generate frequency-selective recoupling as previously described. Decay curves for V9 and P11 carbonyl sites were detected through one-dimensional ^{13}C NMR signals of V9 C_α and P11 C_α, which were polarized by a 2.4 ms period of finite-pulse radio-frequency-driven recoupling (fpRFDR) mixing (6, 7) after the frequency-selective recoupling period of the ^{13}C-BARE sequence. ^{13}C-BARE data were acquired in 7 h, using a 0.8 s recycle delay.

2D ^{13}C-^{13}C and ^{15}N-^{13}C spectra of samples IX and X were acquired with standard methods. For 2D ^{13}C-^{13}C spectra in Figs. 2, 3, and S4, mixing periods used spin diffusion and radio-frequency-assisted diffusion/dipolar-assisted rotational resonance (RAD/DARR), respectively (8, 9). 2D spin diffusion spectra in Fig. 2 were acquired at 187.8 MHz ^{13}C NMR frequency with 17.00 kHz MAS, 104 kHz ^{1}H decoupling, a maximum t_1 period of 6.509 ms, a 200 ms mixing period, a 0.8 s recycle delay, and a total measurement time of 15 h. 2D RAD spectra in Figs. 3 and S4 were acquired at 100.8 MHz ^{13}C NMR frequency with 9.00 kHz MAS, 90 kHz ^{1}H decoupling, a maximum t_1 period of 5.08 ms, 25 ms (Fig. S4a) or 500 ms (Fig. S4b) mixing periods, a 0.5 s recycle delay, and a total measurement time of 3.4 h (Fig. S4a) or 46 h (Fig. S4b).

2D solid state NMR data were processed with NMRPipe (10). Contour levels in contour plots increase by successive factors of 1.5 unless otherwise noted.

Simulations of solid state NMR data

Simulations were performed with programs written specifically for this purpose. PITHIRDS-CT and REDOR simulations used a set of Python routines that included the full time-dependent nuclear spin Hamiltonian under MAS and radio-frequency pulse sequences. REDOR simulations shown in Figs. 3a and S2a included two spins (representing the ^{15}N and ^{13}C labels) with internuclear distances taken from the central four molecules of the final calculated bundle of structures (Fig. S6c). PITHIRDS-CT curves shown in Figs. 3b (left) and S2d included all eight spins (representing the ^{13}C labels) from the structural models.

Five-spin simulations were used for the calculated PITHIRDS-CT curves shown in Figs. 3b (right) and S2e. Since these experiments were performed on samples containing random 1:1 mixtures of MAX1 molecules with ^{13}C labels at either V16 or VX (X = 1, 3, 5, or 7), the simulations were averaged over configurations (as well as over the 20 structures within the final bundle, and over orientations) as follows: (i) Atomic coordinates were taken from the central four molecules of the structural model. The first spin was placed at the carbonyl carbon position of either a V16 or a VX residue in one of the central β-strands of one of the MAX1 molecules; (ii) A series of simulations was run with one spin on each of the three remaining molecules, at either a V16 or a VX carbonyl site. All 16 combinations were considered; (iii) To account for couplings to natural-abundance ^{13}C, the fifth spin was placed 9.0 Å away from the first spin and maximally distant from the other three labeled sites. The choice of a 9.0 Å distance was guided by simulations which showed that this distance produces signal decays nearly identical to those observed in PITHIRDS-CT experiments on unlabeled samples or on samples with dilute carbonyl labels. (iv) Only the first spin was polarized initially, and signals from all spins were detected.

^{15}N-BARE and ^{13}C-BARE simulations were performed as previously described (5). ^{15}N-BARE simulations included either two (for V9, P11, and K13) or three (for T12) ^{15}N spins and were used to generate either ^{15}N-^{15}N distance restraints or a three-dimensional (3D) torsion angle potential surfaces for structure calculations. ^{13}C-BARE simulations included three ^{13}C spins and were used to generate 3D torsion angle potential surfaces. The 3D surfaces were proportional to the χ^2 deviations between experimental and simulated data, as functions of the three torsion angles included in the simulations (namely, ψ_{k-1}, ϕ_k, and ψ_k for ^{15}N-BARE data or ϕ_k, ψ_k, ϕ_{k+1} for ^{13}C-BARE data of residue k).

Electron microscopy

Micrographs of diluted hydrogel samples were obtained using a Hitachi H-7650 transmission electron microscopy at a voltage of 80 kV. Fibrils imaged by TEM were prepared as follows. Samples were prepared the night before each TEM experiment was to occur. For the sample designed to mimic the ssNMR lyophilized hydrogel preparation, 4 wt % peptide stock solutions in water were prepared. Gelation was initiated with an equal volume of buffer composed of 250 mM BTP and 20 mM NaCl at pH 9. The resulting 2 wt% gel was incubated at room temperature for 2 hours. Hydrogels were then frozen by liquid nitrogen and lyophilized. The following day, lyophilized gels were reconstituted with water, an aliquot of the rehydrated gel was removed, diluted 40X with water and mixed thoroughly. Nascent fibrils were prepared from a solution of 300 μM MAX1 in buffer containing 125 mM BTP 10 mM NaCl at pH 9. This solution was incubated overnight at room temperature. For the TEM experiments, 2 μL of the fibril solution and diluted gel were added to 200 mesh carbon coated copper grids with excess liquid blotted away with filter paper. 1 % uranyl acetate solution was then added to the grids as a negative stain to enhance image contrast. Excess stain was blotted away and the grids were imaged immediately.

Structure calculations

Experimentally-based restraints used in structure calculations are listed in Table S2. A structural model for MAX1 fibrils was generated in two stages. In the first stage, starting from a set of eight well-separated copies of MAX1 (without C-terminal amidation), Xplor-NIH (11) was used to generate an idealized, energy-minimized model *in vacuo*. Xplor-NIH calculations included torsion angle potentials (CDIH terms), interatomic distance potentials (NOE terms), three-dimensional torsion angle potential surfaces to represent ^{15}N-BARE and ^{13}C-BARE restraints (TorsionInterpolPot terms), distance symmetry potentials (DistSymmPot terms) that enforced translational symmetry within each of the two β-sheet layers and two-fold rotational symmetry between the two layers, non-crystallographic symmetry potentials (PosDiffPot terms) that enforced identical conformations for all eight MAX1 molecules, and a torsion angle database potential (torsionDBPot term). CDIH terms had force constants of 300 kcal/mol-rad^2. NOE terms had force constants that increased from 1 to 30 kcal/mol-Å^2 during annealing. ^{15}N-BARE and ^{13}C-BARE potential surfaces had force constants of 50 kcal/mol per χ^2 unit. In each independent Xplor-NIH run, the conformation of each MAX1 molecule was first randomized. Torsion angles restrained by CDIH terms were then set within their minimum-energy ranges. After a period of molecular dynamics in torsion angle space at 2000 K, annealing was performed from 2000 K to 10 K in torsion angle space, followed by energy minimizations in torsion angle space and Cartesian space. Forty independent Xplor-NIH runs were performed, leading to eight final low-energy structures with no violations of NOE restraints. These structures were all very similar to one another (2.08 Å rmsd of backbone coordinates of relative to the average backbone coordinates).

The lowest-energy structure from Xplor-NIH calculations was used as the starting point for the second stage, which was carried out with the VMD and NAMD programs (12). First, within VMD, C-terminal amide groups were added to all MAX1 molecules. The MAX1 octamer was then solvated in a box of water molecules. Na^+ and Cl^- ions were added within VMD to approximate 150 mM ionic strength with charge neutrality. The final system contained 1654 water molecules, 5 Na^+ ions, 77 Cl^- ions, and 8 MAX1 molecules in a 80.7 nm^3 volume. A constant-pressure Langevin dynamics simulation was then run for 8.0 ns at 310 K and one

atmosphere, with periodic boundary conditions, particle mesh Ewald electrostatics, the CHARMM27 potential, TIP3P water, and a 2.0 fs time step. During this simulation, structural restraints based on solid state NMR data were enforced as follows: (i) Prior to each 200 fs simulation segment, the current state of the NAMD simulation was stored with a "checkpoint" instruction and the atomic coordinates were written to a PDB file. An external program was then called to evaluate the total (unitless) restraint "energy" E_{rest} for these atomic coordinates, using force constants of 1000.0/Å^2 for distance restraints from REDOR data, 5000.0/Å^2 for distance restraints from ^{15}N-BARE data, 100.0/Å^2 for distance restraints from 2D RAD data, 0.50/deg^2 for torsion angle restraints, and 20.0 per χ^2 unit for 3D ^{15}N- and ^{13}C-BARE restraints; (ii) After each 200 fs segment, the atomic coordinates were again written to a PDB file, the new value of E_{rest} was calculated by the external program, and the change in restrain energy ΔE_{rest} was determined; (iii) The quantity $q_{rest} = \exp(-\Delta E_{rest}/T_{rest})$ was calculated, where T_{rest} was a (unitless) restraint "temperature". Following the standard Metropolis Monte Carlo algorithm, the evolution of atomic coordinates during the 200 fs segment was then either accepted or rejected (via the NAMD "revert" instruction), depending on whether q_{rest} was greater than or less than a random number chosen from the interval from 0.0 to 1.0; (iv) All atomic velocities were then randomized (via the NAMD "reinitvels" instruction), and the next 200 fs simulation segment was initiated; (5) During the 8.0 ns simulations, T_{rest} was decreased from 1280 to 280. The fraction of accepted simulation segments decreased from 0.60 to roughly 0.04 from the beginning to the end of these simulations.

Final structures from stage 1 and stage 2 of the structure calculations are compared in Fig. S7a. Due to the symmetry restraints in the Xplor-NIH calculations, the final structure from stage 1 had nearly identical conformations for all MAX1 molecules and nearly perfect translational symmetry along the fibril growth axis, with a left-handed twist of about 5°/nm about the growth axis. Hydrogen-bonding geometries were clearly non-ideal, since hydrogen bonds were not included explicitly in the Xplor-NIH calculations. Moreover, β-hairpins in the two β-sheet layers were positioned directly above or below one another, with no “staggering” or interdigitation of valine sidechains in the hydrophobic core.

Structures generated in stage 2 were more realistic, since the NAMD simulations did not include symmetry restraints and did include solvation and electrostatic interactions. Molecular conformations in structures from stage 2 were more variable, with greater disorder at the N- and C-termini, in the β-turn, and in sidechains. The left-handed twist increased to about 10°/nm. Hydrogen-bonding geometries improved. Interdigitation of valine sidechains developed in the hydrophobic core. We believe these structures more accurately represent the true structural state of MAX1 fibrils at instants in time. The Monte Carlo algorithm described above ensured that experimentally-based restraints remained in force during stage 2, so these structures are still restrained by the full set of solid state NMR data.

As shown in Fig. S7b, the rmsd of atomic coordinates stabilized to approximately 0.6 Å for backbone atoms and 0.8 Å for all non-hydrogen atoms of the central four MAX1 molecules after roughly 4.0 ns. Coordinates for MAX1 molecules in twenty equally-spaced time points from the final 4.0 ns have been deposited in the Protein Data Bank as file 2N1E. These twenty structures are superimposed in Fig. S7c. Coordinate rmsd values for MAX1 molecules in these structures are 0.51 Å for backbone atoms and 0.89 Å for all non-hydrogen atoms, relative to the average coordinates.

References for Supporting Methods

1. Gullion T & Schaefer J (1989) Rotational-echo double-resonance NMR. *J. Magn. Reson.* 81:196-200.
2. Anderson RC*, et al.* (1995) Conformation of [1-^{13}C,^{15}N]acetyl-l-carnitine: Rotational-echo double-resonance nuclear magnetic resonance spectroscopy. *J. Am. Chem. Soc.* 117:10546-10550.
3. Petkova AT & Tycko R (2002) Sensitivity enhancement in structural measurements by solid state NMR through pulsed spin locking. *J. Magn. Reson.* 155:293-299.
4. Tycko R (2007) Symmetry-based constant-time homonuclear dipolar recoupling in solid state NMR. *J. Chem. Phys.* 126.
5. Hu KN, Qiang W, Bermejo GA, Schwieters CD, & Tycko R (2012) Restraints on backbone conformations in solid state NMR studies of uniformly labeled proteins from quantitative amide ^{15}N-^{15}N and carbonyl ^{13}C-^{13}C dipolar recoupling data. *J. Magn. Reson.* 218:115-127.
6. Ishii Y (2001) ^{13}C-^{13}C dipolar recoupling under very fast magic angle spinning in solid state nuclear magnetic resonance: Applications to distance measurements, spectral assignments, and high-throughput secondary-structure determination. *J. Chem. Phys.* 114:8473-8483.
7. Bennett AE*, et al.* (1998) Homonuclear radio-frequency-driven recoupling in rotating solids. *J. Chem. Phys.* 108:9463-9479.
8. Morcombe CR, Gaponenko V, Byrd RA, & Zilm KW (2004) Diluting abundant spins by isotope edited radio frequency field assisted diffusion. *J. Am. Chem. Soc.* 126:7196-7197.
9. Takegoshi K, Nakamura S, & Terao T (2001) ^{13}C-^{1}H dipolar-assisted rotational resonance in magic-angle spinning NMR. *Chem. Phys. Lett.* 344:631-637.
10. Delaglio F*, et al.* (1995) NMRpipe: A multidimensional spectral processing system based on Unix pipes. *J. Biomol. NMR* 6:277-293.
11. Schwieters CD, Kuszewski JJ, & Clore GM (2006) Using Xplor-NIH for NMR molecular structure determination. *Prog. Nucl. Magn. Reson. Spectrosc.* 48:47-62.
12. Phillips JC*, et al.* (2005) Scalable molecular dynamics with NAMD. *J. Comput. Chem.* 26:1781-1802.

Table S1: NMR chemical shifts in MAX1 fibrils and TALOS+ torsion angle predictions. ^{13}C shifts are relative to 2,2-dimethyl-2-silapentane-5-sulfonic acid (DSS). ^{15}N shifts are relative to liquid ammonia. Only predictions for L-amino acids classified as "good" by TALOS+ are included, with uncertainties equal to twice the values reported by TALOS+.

residue	CO	C_α	C_β	C_γ	C_δ	C_ε	backbone N	sidechain N	ϕ	ψ
V1	177.1	63.1	36.3	21.6						
K8	174.2	54.4	36.0	25.1	29.7	42.4	125.3			
V9	172.4	58.1	32.9	20.9			124.0		-128±40	135±62
$^{D}P10$	174.9									
P11	175.9	63.1	32.1	25.9	49.9		132.9		-68±18	
T12	172.5	63.1	68.9	21.5			118.1			
K13	174.2	54.4	36.0	25.1	29.7	42.4	125.3		-114±66	148±34
V20	177.5	60.3	33.0	20.9			123.8			

Table S2: Restraints used in Xplor-NIH (stage 1) and molecular dynamics/Monte Carlo (stage 2) structure calculations

type of restraint	site, torsion angle, or atom pair	number per MAX1 molecule	comments
TALOS+ torsion angle predictions	ϕ,ψ of V9; ϕ of P11; ϕ,ψ of K13	5	Values in Table S1.
Other torsion angle restraints	ϕ,ψ of residues 1-8 and 14-20	28	Set to ϕ = -135°±30° and ψ = 135°±30° to enforce β-strands. Supported by experimental ^{13}C chemical shifts of backbone carbonyl sites (Fig. S1b). Used only in stage 1.
Distances from ^{15}N-BARE	K8 N to V9 N; P11 N to T12 N	2	Data in Fig. S2b.
Distances from 2D RAD	V20 C_β to T12 C_γ	1	Intermolecular distances between β-sheets. Set to 6.0±2.0 Å. Data in Fig. S5.
3D torsion angle surface from ^{15}N-BARE	T12	1	Restrains ϕ,ψ of T12 and ψ of P11. Data in Fig. S2b.
3D torsion angle surfaces from ^{13}C-BARE	V9, P11	2	Restrains ϕ,ψ of V9 and ϕ of P10; ϕ,ψ of P11 and ϕ of T12. Data in Fig. S2c.
Distances from ^{15}N-^{13}C REDOR	V1 C to V20 N; V3 C to V18 N; V5 C to V16 N; V7 C to V14 N	4	Intramolecular distances. Data in Fig. S2a.
Distances from ^{13}C-^{13}C PITHIRDS-CT	V5 C to V16 C	1	Intermolecular distances for neighboring molecules within a β-sheet. Data in Fig. S2e.
Other intermolecular distances	K2 C to K19 N; K4 C to K17 N; K6 C to K15 N; K8 C to K13 N.	4	Set to 4.3±0.1 Å to represent intermolecular hydrogen bonds between neighboring molecules in the same β-sheet. Supported by experimental ^{13}C-^{13}C PITHIRDS-CT data in Fig. S2d. Used only in stage 1.

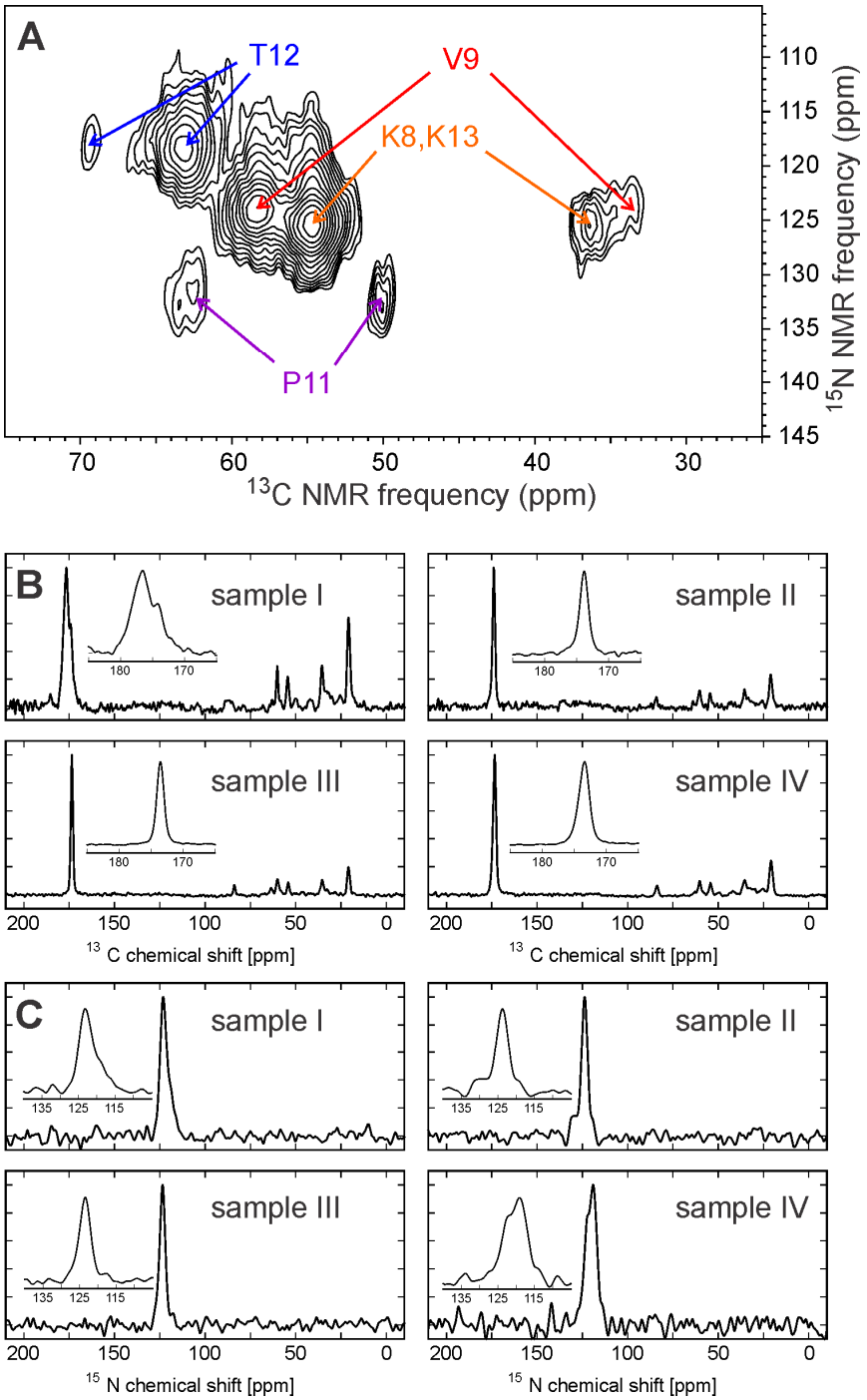

Figure S1: (A) 2D ^{15}N-^{13}C$_\alpha$ spectrum of MAX1 sample IX as a lyophilized gel, obtained at 100.4 MHz ^{13}C NMR frequency with 9.00 kHz MAS. Contour levels increase by successsive factors of 1.3. (B) 1D solid state ^{13}C NMR spectra of samples I-IV. (C) 1D solid state ^{15}N NMR spectra of samples I-IV. Insets in panels B and C show expansions of the carbonyl and amide nitrogen regions of the spectra.

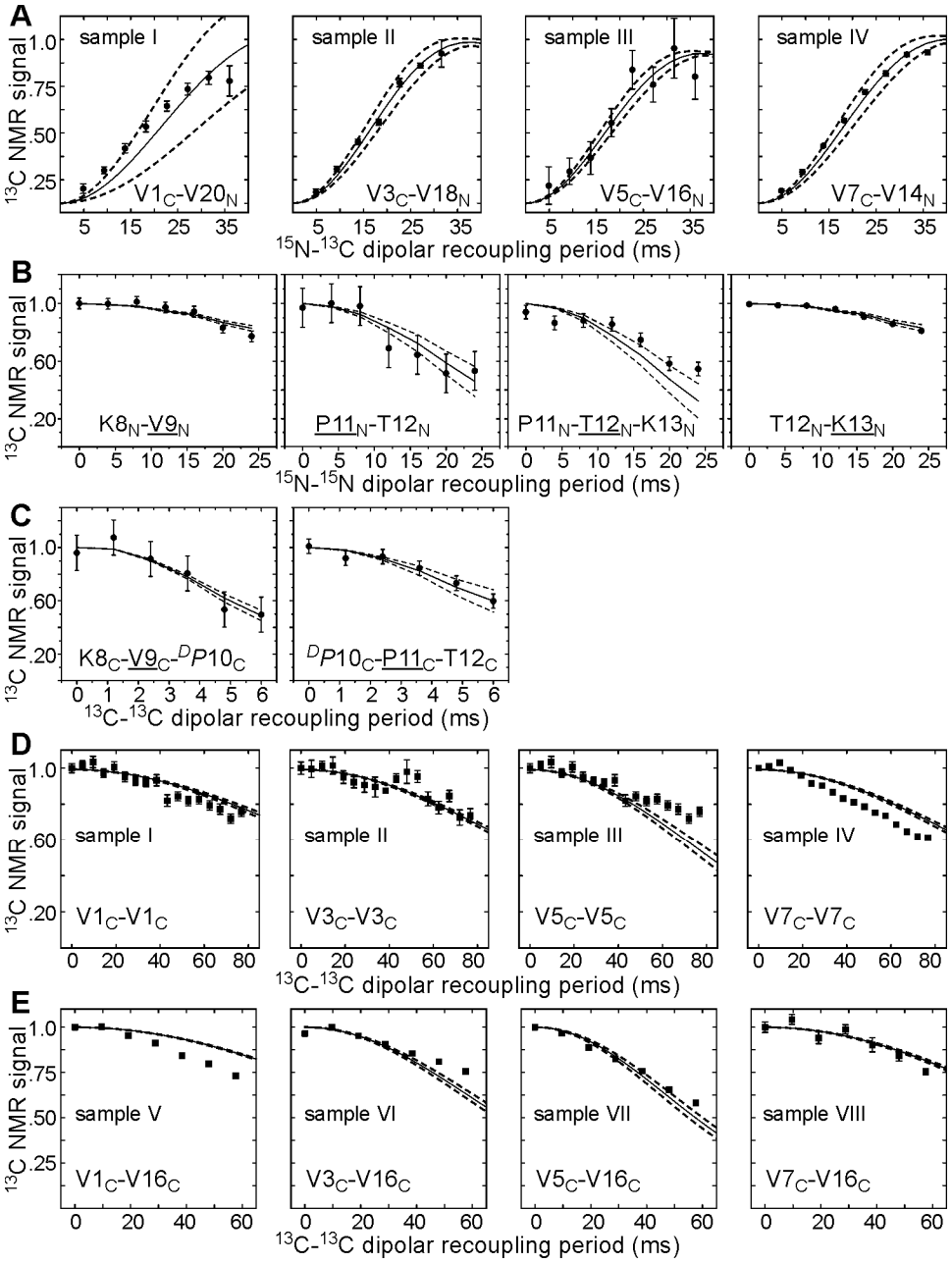

Figure S2: (A) ^{15}N-^{13}C REDOR data from samples I-IV. (B) ^{15}N-BARE data from sample IX. (C) ^{13}C-BARE data from sample IX. (D) ^{13}C PITHIRDS-CT data from samples I-IV. (E) ^{13}C PITHIRDS-CT data from samples I-IV with sample V. The relevant residues and labels are indicated in each panel (C for backbone carbonyl ^{13}C, N for backbone amide ^{15}N). The detected sites in BARE data are underlined. Solid lines in all panels are averaged simulations using atomic coordinates from the final ensemble of 20 MAX1 fibril structures (see text and Fig. S7C), with dashed lines indicating one standard deviation. Error bars on experimental data points represent uncertainties due to the root-mean-squared noise in the solid state NMR spectra.

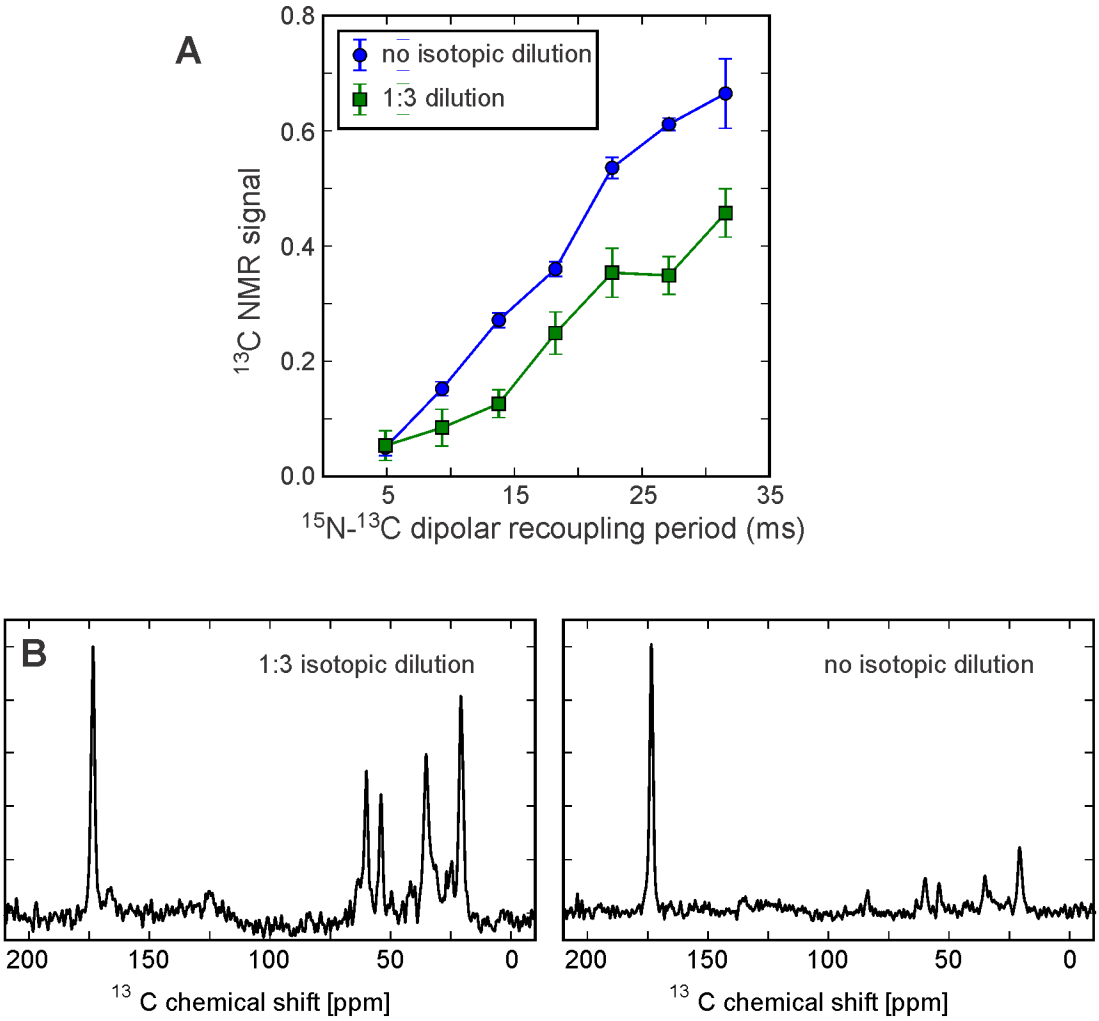

Figure S3: (A) Comparison of ^{15}N-^{13}C REDOR data for MAX1 fibrils with the labeling pattern of sample II, with and without dilution in unlabeled molecules. REDOR $\Delta S/S_0$ signals are plotted without rescaling. The lower values for the diluted sample are attributable to the larger contribution from natural-abundance ^{13}C signals to S_0. (B) Comparison of 1D ^{13}C NMR spectra of diluted and undiluted samples.

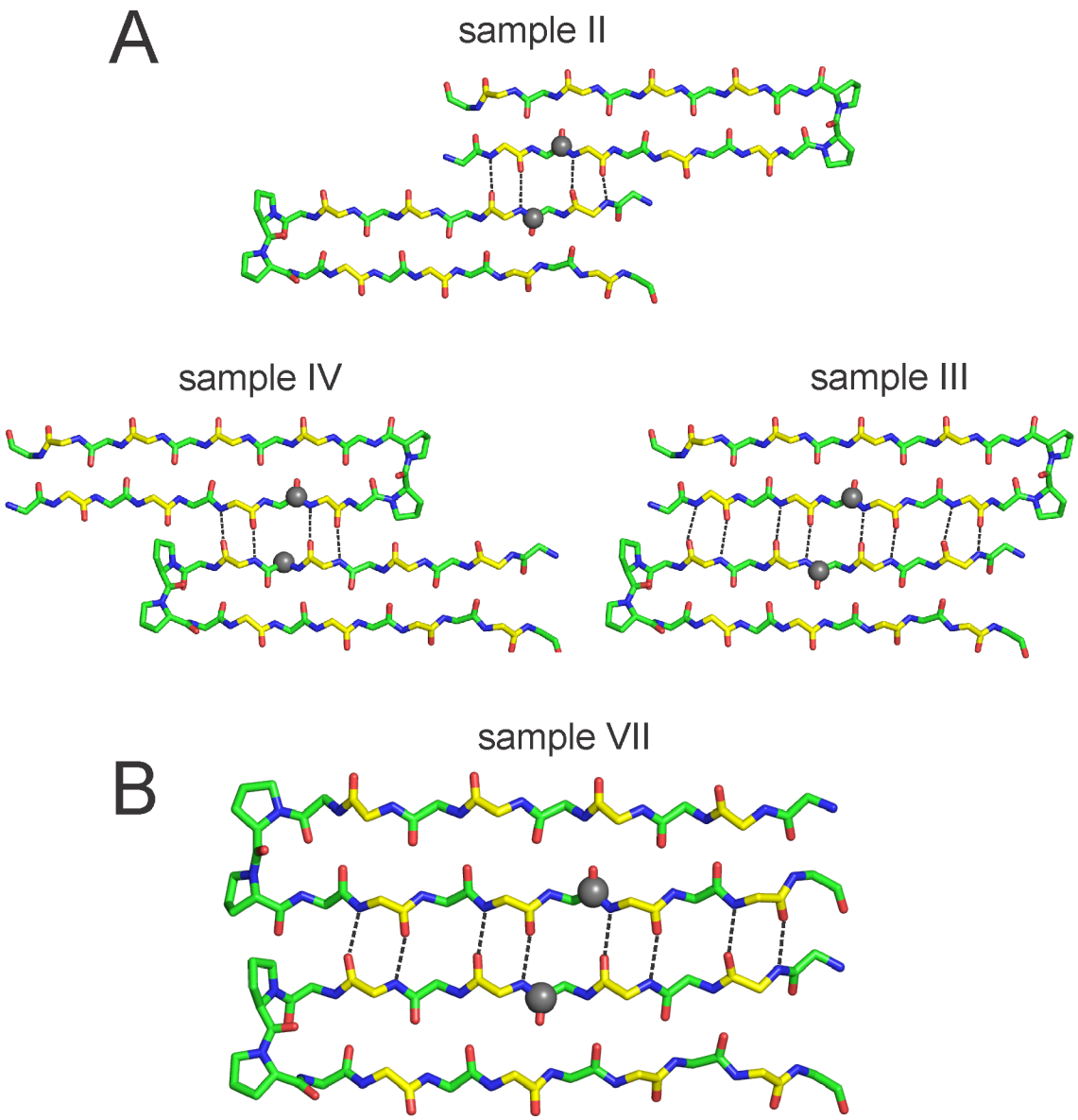

Figure S4. Strategy for determining β-sheet structure in MAX1 fibrils. (A) If β-hairpins assembled into β-sheets with an *Anti* configuration, a short intermolecular distance between ^{13}C labels (grey balls) would be observed in PITHIRDS-CT data for sample II, sample III, or sample IV. The three possible registries of intermolecular hydrogen bonds (dashed lines) between neighboring MAX1 molecules that would produce ^{13}C-^{13}C distances of approximately 6.1 Å for these samples are shown, with carbon atoms in lysine residues colored yellow. In fact, the PITHIRDS-CT data in Fig. S2D indicate longer ^{13}C-^{13}C distances in all three samples. (B) The short ^{13}C-^{13}C distance observed for sample VII in Fig. S2E supports a *Syn* configuration with the indicated registry, for which intermolecular hydrogen bonds can form between lysine residues n and 19-n, with n = 0, 2, 4, and 6.

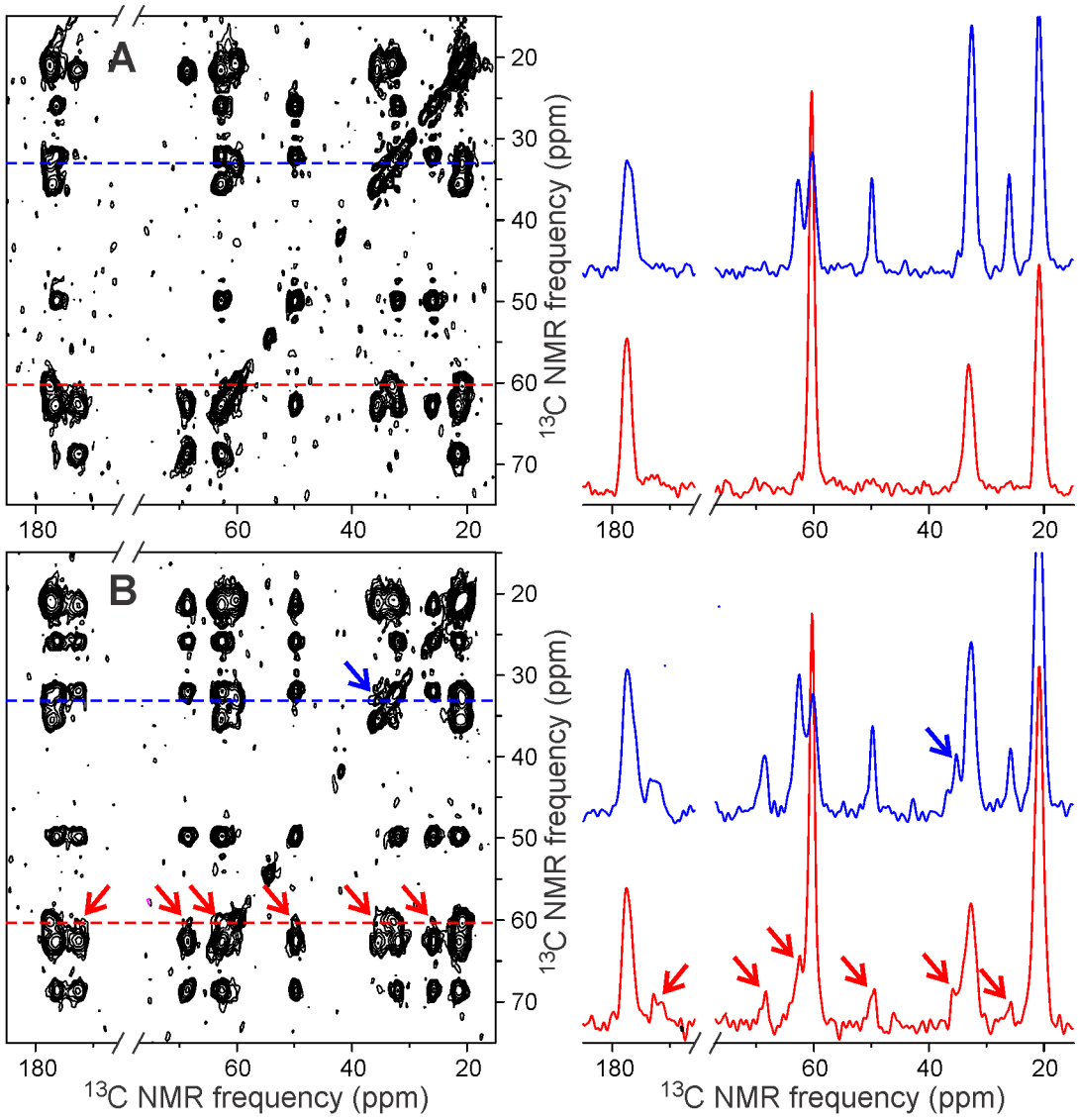

Figure S5: 2D solid state ^{13}C-^{13}C NMR spectra of sample X with RAD mixing periods of 25 ms (A) and 500 ms (B), with 1D slices at C_α (red) and C_β (blue) chemical shifts of V20. Arrows indicate long-range inter-residue crosspeaks that serve as restraints on supramolecular structure in MAX1 fibrils. Spectra were obtained at 100.8 MHz ^{13}C NMR frequency with 9.00 kHz MAS. The lyophilized MAX1 gel sample was rehydrated in the MAS rotor before these measurements.

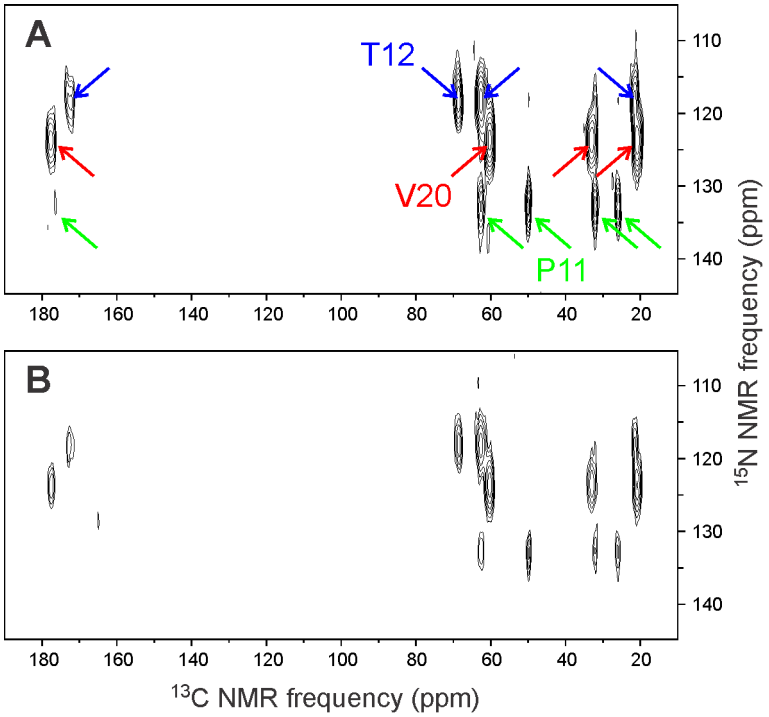

Figure S6: (A) 2D ^{15}N-^{13}C spectrum of MAX1 sample X as a rehydrated gel, with crosspeak assignments. The spectrum was obtained at 100.4 MHz ^{13}C NMR frequency with 9.00 kHz MAS, using a 4.0 ms frequency selective ^{15}N-$^{13}C_{\alpha}$ cross-polarization period and a 2.67 ms period of ^{13}C-^{13}C mixing under fpRFDR between the t_1 and t_2 periods. (B) 2D ^{15}N-^{13}C spectrum of MAX1 sample XI under the same conditions. Comparison of these spectra confirms the chemical shift assignments for V20 in Fig. 3C, Fig. S5, and Table S1.

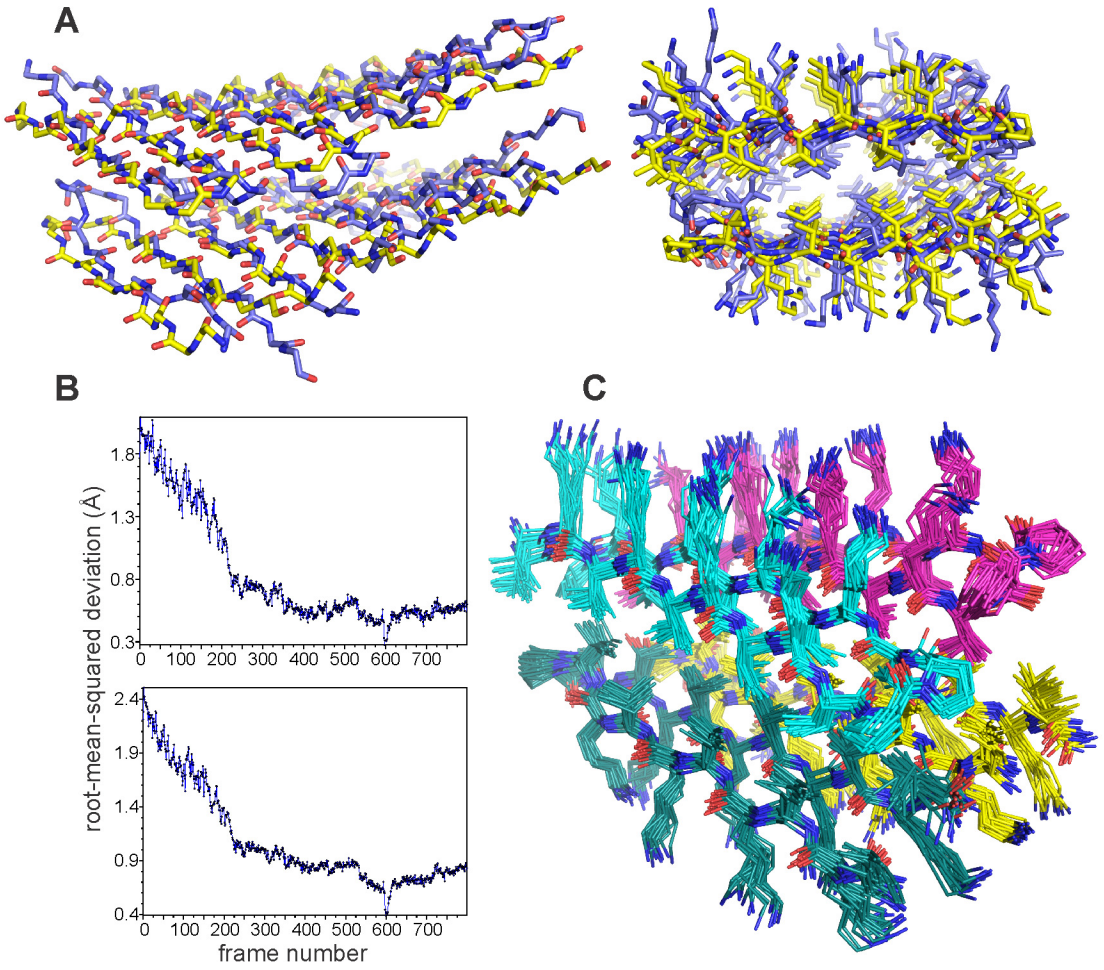

Figure S7: (A) Superposition of the idealized structural model obtained with Xplor-NIH calculations (yellow carbon atoms) and the final structural model obtained with molecular dynamics/Monte Carlo calculations (blue carbon atoms). The Xplor-NIH model was used as the starting point for the subsequent molecular dynamics/Monte Carlo calculations. The superposition is viewed with the fibril growth axis perpendicular to the page (right) and at an oblique angle (left). (B) Atomic coordinate rmsd values during the molecular dynamics/Monte Carlo calculations, relative to the coordinates at frame 600, for backbone atoms (top) and all non-hydrogen atoms (bottom) of the central four MAX1 monomers. (C) Superposition of structures from 20 equally spaced frames from the final half of the molecular dynamics/Monte Carlo trajectory. Only the central four MAX1 monomers are shown, with carbon atoms of different monomers colored cyan, magenta, teal, or yellow for clarity. This set of structures was used in the simulations of NMR data shown in Figs. 3 and S2.

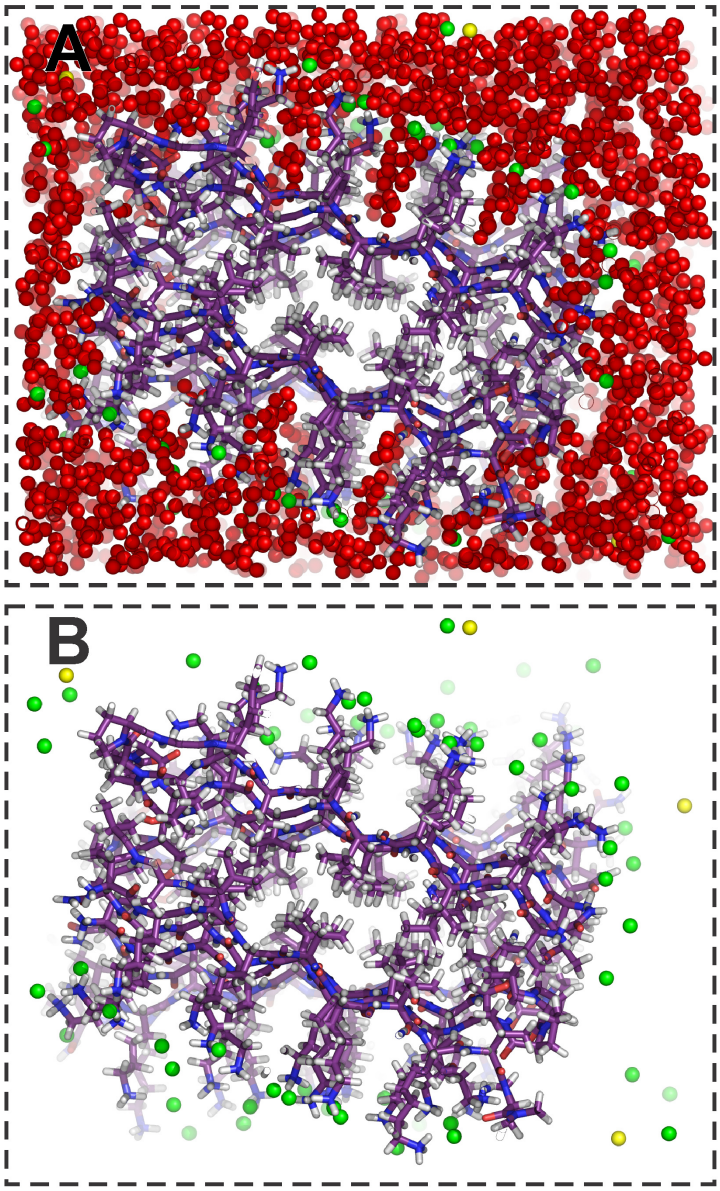

Figure S8: Solvation of final MAX1 fibril structure from molecular dynamics/Monte Carlo calculations. (A) Final frame from structure calculations, showing MAX1 molecules as a stick representation with carbon atoms in purple, oxygen atoms of water molecules as red spheres, chloride ions as yellow spheres, and sodium ions as green spheres. The hydrophobic fibril core contains no water molecules or ions. Lysine sidechains are fully solvated on the exterior of the fibril. (B) Same representation, but with water molecules removed to show the partial association of choride ions with amine groups on lysine sidechains.